
# Customized and high-performing acoustic levitators for contact-free experiments

Journal of Science: Advanced Materials and Devices 9 (2024) 100720

Contents lists available at ScienceDirect

Journal of Science: Advanced Materials and Devices

journal homepage: www.elsevier.com/locate/jsamd

# Customized and high-performing acoustic levitators for contact-free experiments

Smaragda-Maria Argyri [a], Carl Andersson [b], Nicolas Paillet [a], Lars Evenäs [a], Jens Ahrens [b], Asier Marzo [c,**], Víctor Contreras [d,***], Romain Bordes [a,*]

[a] Department of Chemistry and Chemical Engineering, Chalmers University of Technology, 41296, Gothenburg, Sweden
[b] Division of Applied Acoustics, Chalmers University of Technology, 41296, Gothenburg, Sweden
[c] UPNA Lab, Department of Mathematics and Computer Engineering, Public University of Navarra, Pamplona, Navarra, 31006, Spain
[d] Instituto de Ciencias Físicas, Universidad Nacional Autónoma de México, Cuernavaca, 62210, Mexico

ARTICLE INFO

*Keywords:*
Customized design
Multiple-transducers
Acoustic levitator
Contact-free

ABSTRACT

Acoustic levitators are becoming increasingly common research instrumentation for contact-free, lab-in-a-droplet studies. Recently, levitators that employ multiple, small, ultrasonic transducers have gained popularity, given their low price, temperature and spatial stability, low voltage, and accessibility. Yet, the current state-of-the-art device, TinyLev, presents limitations for certain applications in terms of stability, strength, and compactness. Herein, we developed three new levitators and evaluated the effect of the construction parameters (*e.g.*, distance of opposing arrays, number and arrangement of transducers, *etc.*) on their performance. The best performing levitator from this work had half the number of transducers, compared to TinyLev, though presented 1.7 and 3.5 times higher levitation capacity along the horizontal and vertical configurations, respectively, and 4.7 and 2.0 times higher horizontal and vertical stability of a levitated object, respectively. Additionally, we present a direct means to evaluate the acoustic radiation net force acting on a deformable object for uniaxial levitators, without the use of a microphone or a schlieren deflectometer for this type of levitators. The theoretical and experimental observations provide insights for adapting the acoustic levitator design for specific applications. Finally, we developed an open-source software which allows the evaluation of the acoustic pressure field generated by customized designs and provides the necessary files for 3D printing the scaffold of the levitator. This study aims to increase accessibility and promote further developments in contact-free experiments.

## 1. Introduction

The ability to levitate objects with ultrasonic standing waves ($f \geq 20$ kHz) has been widely explored due to its scientific potential and technological applications where the study of objects in a contact-free manner is central. Compared to other levitation techniques, acoustic levitation occurs regardless of the physical properties of the sample such as its electric, magnetic, or optical response, thus presenting a wide applicability for the study and manipulation of materials in the fields of soft-matter [1–3], chemistry [4–7], and biology [8–11]. The allocation of the sample in mid-air allows the contact-free manipulation and study of dynamic phenomena without the presence of a solid interference and associated shortcomings (*e.g.*, contamination, surfaces induced effects, *etc.*). The main limitation is related to the weight and size of the levitated samples that may restrict its implementation in certain applications.

The acoustic levitation of objects smaller than half the wavelength occurs slightly below the areas with the lowest time-averaged acoustic pressure (*i.e.*, nodes), resulting from the destructive interference of counter-propagating ultrasonic waves. For airborne applications, the ultrasonic wave sources have traditionally been generated by high-power Langevin transducers coupled to mechanical amplifiers, known as horns or sonotrodes [12–14]. The most common configurations are axisymmetric cavities with single transducer-reflector (T-R) and transducer-transducer (T-T) apparatus [13]. Previous parametric studies

Peer review under responsibility of Vietnam National University, Hanoi.
* Corresponding author.
** Corresponding author
*** Corresponding author
*E-mail address:* bordes@chalmers.se (R. Bordes).

https://doi.org/10.1016/j.jsamd.2024.100720
Received 25 October 2023; Received in revised form 9 April 2024; Accepted 12 April 2024
Available online 16 April 2024

on the improvement of the levitation performance for the expansion of its applications to high-density materials (such as mercury and iridium) were mostly performed on T-R levitators [15–17]. However, the reported levitator design presented practical limitations since the field of view in the axial direction (see Fig. 1a), was below 1 cm leading to limited visual access to the levitated samples for further analysis. Furthermore, Langevin horns present a lack of lateral forces (see Fig. S1, Supporting Information), which may lead to difficulty in depositing a sample along with instabilities during operation. In this study, we focused on the levitation of small volume liquid samples (0.5–5 μL), with a diameter below the wavelength of the sound waves. Hence, improvements on levitating larger objects will not be addressed.

In the last decade, Langevin transducers have been replaced by arrays of small (d = 1 cm), off-the-shelf, ultrasonic transducers as the source of ultrasound waves. Besides the benefit of a lower cost and a simpler manufacturing process, these levitators achieve similar, and in some cases higher acoustic forces than the Langevin-based devices with lower power consumption [13]. Moreover, the discretization of the vibrating surface into small elements allows generating a dynamic acoustic field by controlling independently the individual phase of the transducers, enabling the contact-free, spatial manipulation of the levitated objects which can be important in applications related to contact-free self-assembly and mixing of hazardous chemicals [18–20].

The transducer arrangement may vary from planar arrays facing each other in one [21], and two dimensions [22], to arrays with concave geometries (see Fig. 1a). The latter ones allow the generation of stronger trapping forces [23] which is relevant for the levitation of liquid droplets. For the levitation of liquids, the arrays can be focused using different strategies [22,24]. The simplest and most efficient way to focus them is by placing the transducers on a concave arrangement, along an imaginary sphere (see Fig. 1b) [25]. The spherical, concave surface can be geometrically described by the radius of curvature, $r$, which corresponds to the radius of the imaginary sphere, along which the transducers are place, the cavity aperture, $D$, which is the distance between the farthest transducers on the same cavity, and the opening angle, $\theta$ (see Fig. 1b). The most common arrangement of transducers is illustrated in Fig. 1c where the transducers are distributed among three concentric rings. Depending on the chosen arrangement and the presence or on of the plastic transducers casing, the packing density of the transducers, $d_{\text{transd.}}$ can vary. This parameter is calculated from Eq. S(1) to Eq. S(3), in accordance to Fig. S2, Supporting Information.

Recent studies have shown that multiple-transducers, axisymmetric, spherical-like levitators are capable of levitating dense objects. Marzo et al. [25], designed a concentric acoustic cavity (*i.e.*, $L = 2r$), known as TinyLev that is capable of levitating objects with densities up to 6.5 g/cm$^3$. Additionally, it was mentioned that the trapping strength is enhanced by simultaneously reducing the radius of curvature, and distance of opposing arrays of the levitator. Later, it was shown that by optimizing the distance of opposing arrays, $L$ of TinyLev it was possible to levitate metallic samples, with density of up to 13.5 g/cm$^3$, while presenting a sufficiently large field of view for the deposition and monitoring of the levitated objects [26]. Furthermore, one of the designs presented in this study was used for the contact-free determination of surface tension of surfactant solutions. The good performance of the levitator in terms of stability and levitation strength, allowed the generation of a large dataset that was then used to train a machine learning algorithm that successfully correlated the droplet features to the surface tension [7]. Despite the recent developments in using multiple, small transducers for building levitators, the key designing parameters influencing the performance of this type of levitators remain underexplored. Furthermore, the diverse applications of acoustic levitation often require adaptation of the acoustic levitator design. Yet, there are no guidelines that can facilitate the choice of designing parameters for the customization of multiple-transducers acoustic levitators.

Herein, three new designs of acoustic levitators, referred to as Mk1, Mk2, and Mk3, that differed in curvature of radius, cavity aperture, number of transducers, and transducer arrangement are presented. The designs were chosen based on practical considerations. Initially, the acoustic pressure and acoustic radiation force fields of each levitator was simulated through the theoretical framework by Andersson [27]. Following, their performance in terms of levitation strength, stability and acoustic force were experimentally evaluated. Furthermore, we built an interactive, open-source software where the user can input the desirable designing parameters of an acoustic levitator and the resulting acoustic pressure fields and forces are calculated. With this study, we provide practical guidelines for the design of acoustic levitators that satisfy specific needs, while the open-source software facilitates the design and 3D printing of customized devices.

## 2. Methods

### 2.1. Simulations

All simulation were performed using the Python library *levitate* [28].

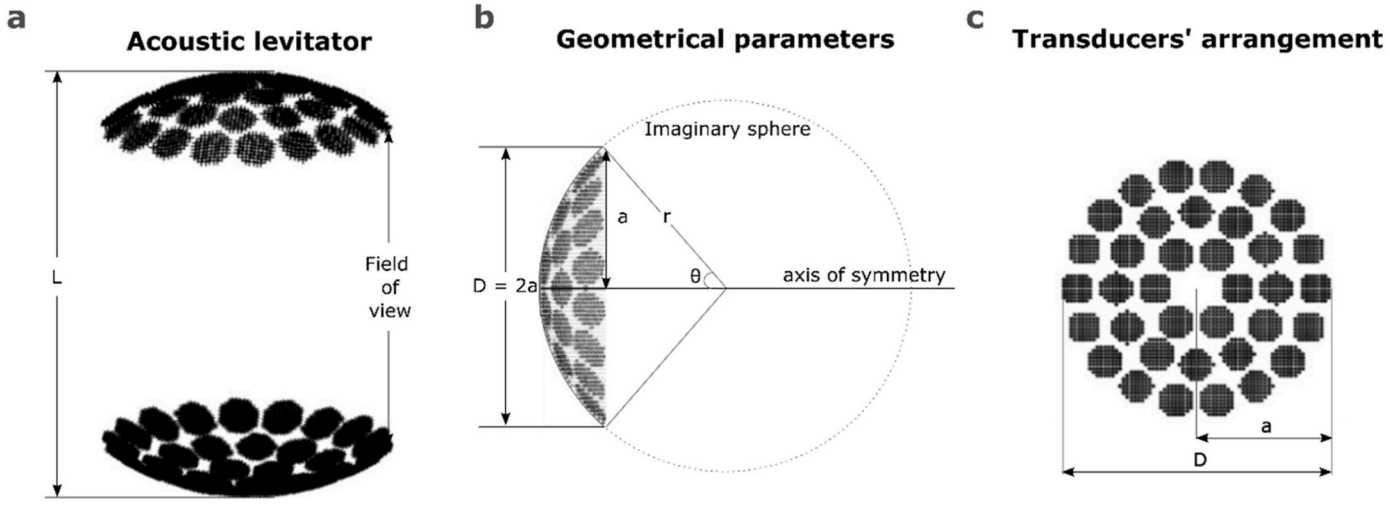


**Fig. 1.** a) Illustration of an axis-symmetric multiple-transducers acoustic levitator, with distance of opposing arrays, $L$, b) geometrical parameters that describe the cavity design, where $D$ and $a$ are the diameters and radius of circular aperture, respectively, $r$ is the radius of curvature that defines the radius of the imaginary sphere the transducers are placed on (dashed line) and $\theta$ is the opening angle from the center of the imaginary sphere, c) illustration of a spherical arrangement of 36 transducers distributed on three concentric rings, which corresponds to the design of TinyLev [15].

The coordinates of the centers of the transducers and the code needed to replicate the simulations can be found on https://git.chalmers.se/bordes/omnilev.

#### 2.1.1. Acoustic pressure field

The simulations of the acoustic pressure fields generated by different transducer configurations are based on the perturbation theory of ultrasonic waves and results from the superposition of the acoustic waves generated by each transducer [29]. The acoustic pressure of a single, point source, transducer, $j$, is given by:

$$p_j = \frac{e^{ikr_j}}{r_j} J_0\left(ka\sin\left(\theta_j\right)\right) \tag{1}$$

where, $r_j$ is the distance between the transducer $j$ and the levitation point, $k$ the wavenumber, $a$ the transducer effective radius, $J_0$ the Bessel function of the first kind and zeroth order, and $\theta_j$ the angle between the observation point and transducer normal.

The directivity pattern of each transducer was set in a circular ring with an effective radius of 3 mm, the operational frequency was set to 40 kHz and the parameter $p_0$, which corresponds to the sound pressure generated by a single transducer at 1 m was arbitrary set to 1 Pa. The values were normalized with respect to the simulated acoustic pressure of Mk3.

#### 2.1.2. Gor'kov potential

We simulated the acoustic radiation force field that is generated when a polystyrene bead with diameter of 1 mm is acoustically levitated from the spatial gradient of the Gor'kov potential:

$$F = -\nabla U \tag{2}$$

where, $U$ is the Gor'kov potential:

$$U = \frac{V}{4}\left(f_1\kappa_0\langle p\rangle^2 - \frac{3}{2}f_2\rho_0\langle v\rangle^2\right) \tag{3}$$

where $V$ is the volume of the particle, $\kappa_0$ is equal to $\rho_0{}^*c_0^2$, $\rho_0$ and $c_0$ are the density of and the speed of sound in the medium (*i.e.*, air), respectively, $\langle p\rangle^2$ and $\langle v\rangle^2$ are the mean square deviations of pressure and velocity respectively, and parameters $f_1$ and $f_2$ are defined as:

$$f_1 = 1 - \frac{\kappa_p}{\kappa_0} \tag{4}$$

and,

$$f_2 = 2\frac{\rho_p - \rho_0}{\rho_p + \rho_0} \tag{5}$$

where, $\kappa_p$ is equal to $\rho_p{}^*c_p^2$, while $\rho_p$ and $c_p$ are the density of and the speec of sound within the levitated particle, respectively.

#### 2.1.3. Acoustic radiation force

The acoustic radiation force applied on a spherical particle with a diameter of 1 mm was calculated from the class levitate.fields.RadiationForce of the Python library *levitate* [28], in accordance with Sapozhnikov and Bailey [30] as formulated in Ref. [27].

#### 2.1.4. Axial trap stiffness

The axial trap stiffness along the horizontal and vertical directions was calculated through the class levitate.fields.RadiationForceGradient [19] at the anti-node. This parameter is correlated to the displacement that the levitated object will experience. The higher the stiffness the more converging the forces will be, thus preventing the displacement of the levitated sample. Hence, the levitator's ability to keep heavier objects aloft is expected to be higher.

### 2.2. Building the acoustic levitators

The scaffolds of the acoustic levitators were designed in OpenScad, and 3D printed (Ultimaker S3, Netherlands) with polylactic acid (PLA). The polarity of the ultrasonic transducers (Manorshi, MSO-P1040H07T) was identified by using an oscilloscope, as described in Ref. [25], and a custom setup. The transducers with the same polarity were wired together. The operating frequency of the transducer was set through an Arduino Uno board at 40 kHz, while the driving signal was then amplified with an L298 N H-bridge. Further information about the transducers used for this study can be found in Ref. [31]. The levitator can operate i) in phase configuration, when all transducers have the same driving signal, and ii) in phase opposition, when a π rad phase difference is applied by driving the two halves using signal in phase opposition. This is done simply by switching the polarity on the two channels of the L298 N amplifier.

### 2.3. Effect of distance of opposing arrays

We levitated single water droplets at a constant operation voltage of 9.5 V, while the levitator halves were simultaneously moved in opposite directions with a step of 0.1 mm in each direction, followed by a 1 s pause. Images were recorded during each step and the contours of the levitated objects were extracted through the Python library OpenCV (see Fig. S3, Supporting Information). The Canny edge detection algorithm [32] and the *findContour* function [33] were applied for that purpose. Videos demonstrating the real-time fitting and the stability of the levitators are available on https://git.chalmers.se/bordes/omnilev. From the contours we determined the center of the droplets and the aspect ratio, while the current consumption of the acoustic levitator was recorded through the Arduino Uno board with an ACS70331 module. The distance of opposing arrays was defined as the distance between the two utmost transducers, as illustrated in Fig. 1a.

### 2.4. Frequency of transducers

The frequency of the ultrasonic transducers was controlled through an Arduino Uno board that controlled an Si5351A (Adafruit) module as a clock generator whose signal was then amplified with an L298 N H-bridge. We varied the operating frequency of the transducers from 36 kHz to 41 kHz and the current consumption was measured on the main line of the circuit using magnetoresistive current sensor module based on an ACS70331 chip, connected to the Arduino board. The Arduino and the power supply were connected to a computer running through the serial port. The circuit is illustrated in Fig. S4, Supporting Information.

Two different array configurations were examined; as single-side independent arrays (see Fig. S10a, Supporting Information) and coupled arrays forming a cavity (see Fig. S10b, Supporting Information). The frequency sweeps were performed at three voltages (7, 10, and 12 V), when the opposing halves were operating either in phase ($\varphi = 0$ rad), or in phase opposition ($\varphi = \pi$ rad). The measurements were repeated three times. The Python codes are available on https://git.chalmers.se/bordes/omnilev.

### 2.5. Levitation capacity

We levitated a solid, spherical, silica bead with known weight, and we gradually reduced the voltage until the bead ceased to levitate, while the opposing, levitator halves were operating in phase opposition. The lowest voltage at which a spherical, silica bead with known weight stopped levitating was recorded in both vertical (normal operational configuration, see Fig. S14a, Supporting Information) and horizontal configuration (see Fig. S14b, Supporting Information). For TinyLev we used a silica bead with a diameter of ~1.38 mm and 1 mg in mass, when operating in horizontal configuration, while for the new designs we used a silica bead with a diameter of ~2.07 mm, and 7 mg in mass. The

measurements were repeated three times, and the standard deviation was calculated. The levitation capacity, $C_{lev}$, of an acoustic levitator was defined as the force of gravity per minimum voltage, $V_{min}$ required to levitate an object of known weight, as:

$$C_{lev} = \frac{mg}{V_{min}}, V_{min} \geq 5 \text{ V} \quad (6)$$

### 2.6. Levitation stability

The spatial stability of the levitators was evaluated with the use of Milli-Q water droplets with volume in the range of 0.5–5 μL, without the presence of setups for damping ambient-vibrations. Specifically, water droplets were levitated, and a digital camera (Basler, model ACA640-750UMAC0, operated at 1 fps) was used to record images over a period of 10 min. The stability was investigated at three different voltages (7 or 7.5 V, 10 V, and 12 V), while the opposing levitator halves were operating in phase opposition. The position and volume of the droplets were monitored and the coordinates of the center of the droplet on the x (horizontal displacement) and z (vertical displacement) axes were determined. The measurements were repeated three times, and the standard deviation was calculated.

## 3. Results and discussion

### 3.1. Designs of customized acoustic levitators

One of the advantages of multiple-transducers acoustic levitator is the design flexibility, since it allows the customization of the device depending on the application. For instance, building a levitator with less transducers increases the compactness of the device, yet the field of view can be sufficiently large for lateral visual access to the levitated sample. Inspired by TinyLev [25], we theoretically and experimentally evaluated three designs of acoustic levitators (*i.e.*, Mk1, Mk2, and Mk3) that were satisfying the demands of practical applications in terms of compactness, stability, and levitation strength.

In Fig. 2, photorealistic renderings of the designed acoustic levitators are shown without the levitator frame. Levitator Mk1 had a radius of curvature equal to 28.1 mm, distance of opposing arrays of 52.2 mm, and consisted of 34 transducers in total with plastic casing, that were concentrically distributed (see Fig. 2a–b). In the case of levitator Mk2 (see Fig. 2c–d), we further increased the compactness by removing the plastic casing of the transducers and placing them closer together in concentric circles. The total number of transducers was 24, while the distance of opposing arrays and the radius of curvature were 38.1 mm and 20.0 mm, respectively. For levitator Mk3 (see Fig. 2e–f), we used 36 transducers, for which the plastic shells were removed, the distance of opposing arrays was 43 mm, and the radius of curvature was 21 mm. The transducers were packed in a hexagonal arrangement; this way the geometrically highest packing density could be achieved. Moreover, the opposing levitator halves were rotated at an angle of 60° with respect to each other, so that the opposing transducers were diagonally facing each other across the central node. The cumulative effect of the packing and the rotation was expected to improve the trapping force of the levitator.

In Table 1, the design parameters are presented. The last column refers to the presence or absence of transducer casing. For practical reasons, the transducers are covered with a plastic case. As mentioned, for acoustic levitators Mk2 and Mk3, this casing was removed to gain space and increase the packing of the transducers.

### 3.2. Simulations of acoustic pressure fields

After choosing the desired design parameters, the acoustic pressure field that each acoustic levitator generates were calculated from Eq. (1). Each transducer was described as a point source with the directivity of a circular piston. Two different scenarios were defined, depending on the phase difference between the acoustic waves produced from the top half

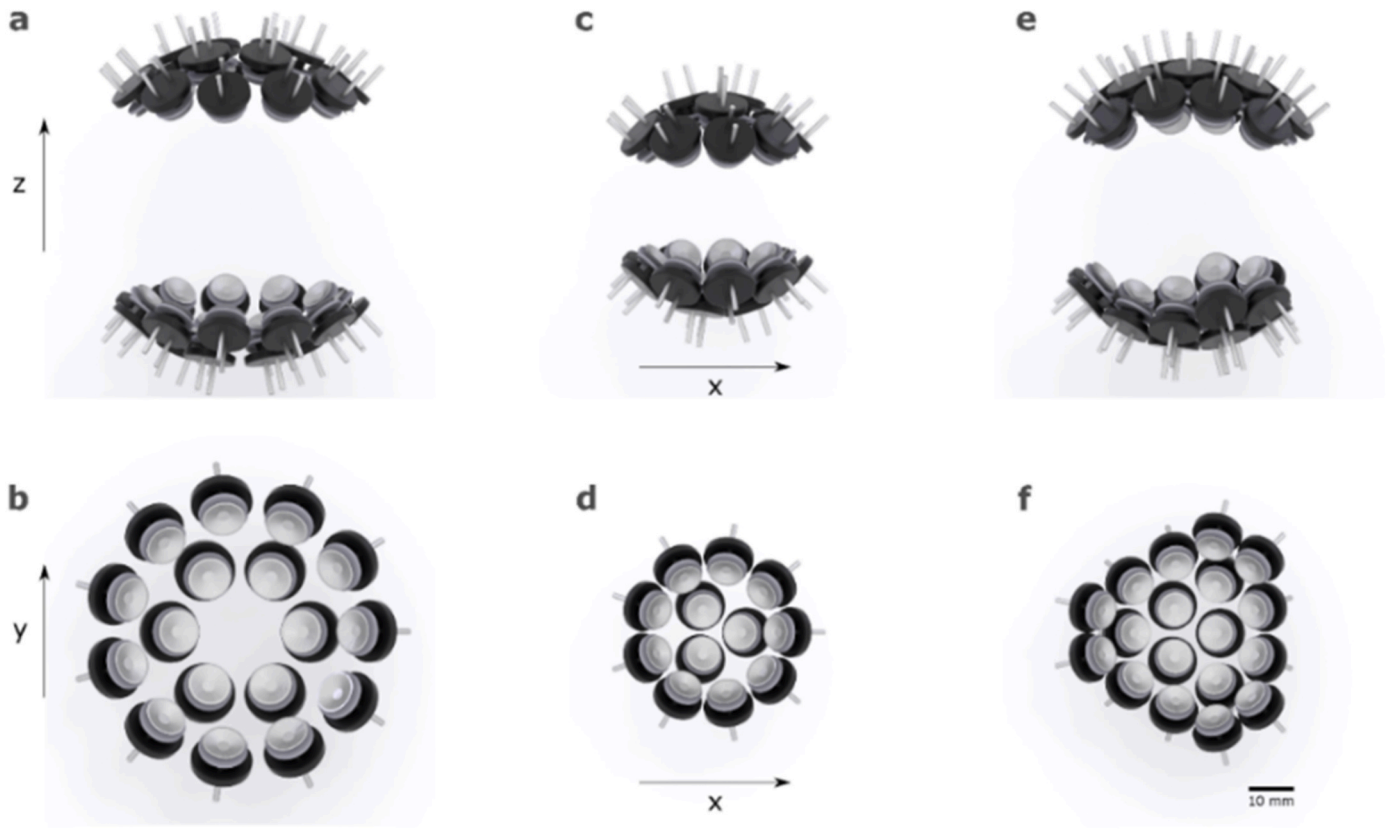


**Fig. 2.** Renderings of acoustic levitators Mk1, Mk2, and Mk3 from the from the (a–c) side view, and (d–f) top view, respectively.

**Table 1**
Structural parameters of the acoustic levitators built and investigated: Mk1, Mk2, and Mk3.

| Levitator | No. of transducers | $L$ (mm) | $f$ (mm) | D (mm) | $r$ (mm) | $\theta$ (°) | $d_{transd.}$ (transd./cm$^2$) | Geom. arrang. | Casing of transd. |
|---|---|---|---|---|---|---|---|---|---|
| TinyLev | 72 | 120 | 106 | 70 | 60 | 41.2 | 1.36 | Concentric | Yes |
| Mk1 | 34 | 52 | 40 | 60 | 28 | 43.0 | 1.73 | Concentric | Yes |
| Mk2 | 24 | 38 | 27 | 36 | 20 | 47.0 | 1.83 | Concentric | No |
| Mk3 | 36 | 43 | 32 | 40 | 21 | 50.0 | 2.42 | Hexagonal | No |

and the bottom half of transducers. In the first case, the transducers had a phase difference of $\varphi = \pi$ rad (*i.e.*, phase opposition) and in the other, there was no phase difference $\varphi = 0$ rad (*i.e.*, in phase). The phase difference affects the wave interactions between the two halves, and as a result the position of the nodes. In Fig. 3, we present the case of phase opposition, where the central node positioned at $z = 0$ and the acoustic pressure is uniformly distributed around that node. This is relevant from a practical perspective, as often only one acoustic node is used for monitoring and manipulating a single-standing droplet. The case of no phase difference is shown in Fig. S5, Supporting Information.

In Fig. 3a–c and Fig. 3d–f, the simulated acoustic pressure fields generated by each acoustic levitator, in the xz and yz planes, respectively, are shown. For levitators Mk1 and Mk2, the acoustic pressure fields in xz and yz planes are similar due to the symmetric spherical arrangement of transducers. However, the hexagonal arrangement of levitator Mk3 with the 60° rotation between the opposing levitator halves, leads to a slightly different acoustic pressure pattern on the xz plane compared to the previous designs. In terms of maximum acoustic pressure, levitator Mk2 presented equally high acoustic pressure to Mk1 (approximately 70% of the maximum acoustic pressure generated by Mk3), despite having less transducers. This is attributed to the shorter distance of opposing arrays for Mk2 in comparison to Mk1, which increases the acoustic pressure around the focal point. Levitator Mk3 presented the highest acoustic pressure, according to the simulations. From the packing density calculations, we observe that Mk3 is more densely packed than Mk1, and Mk3, by approximately 33% and 28%,

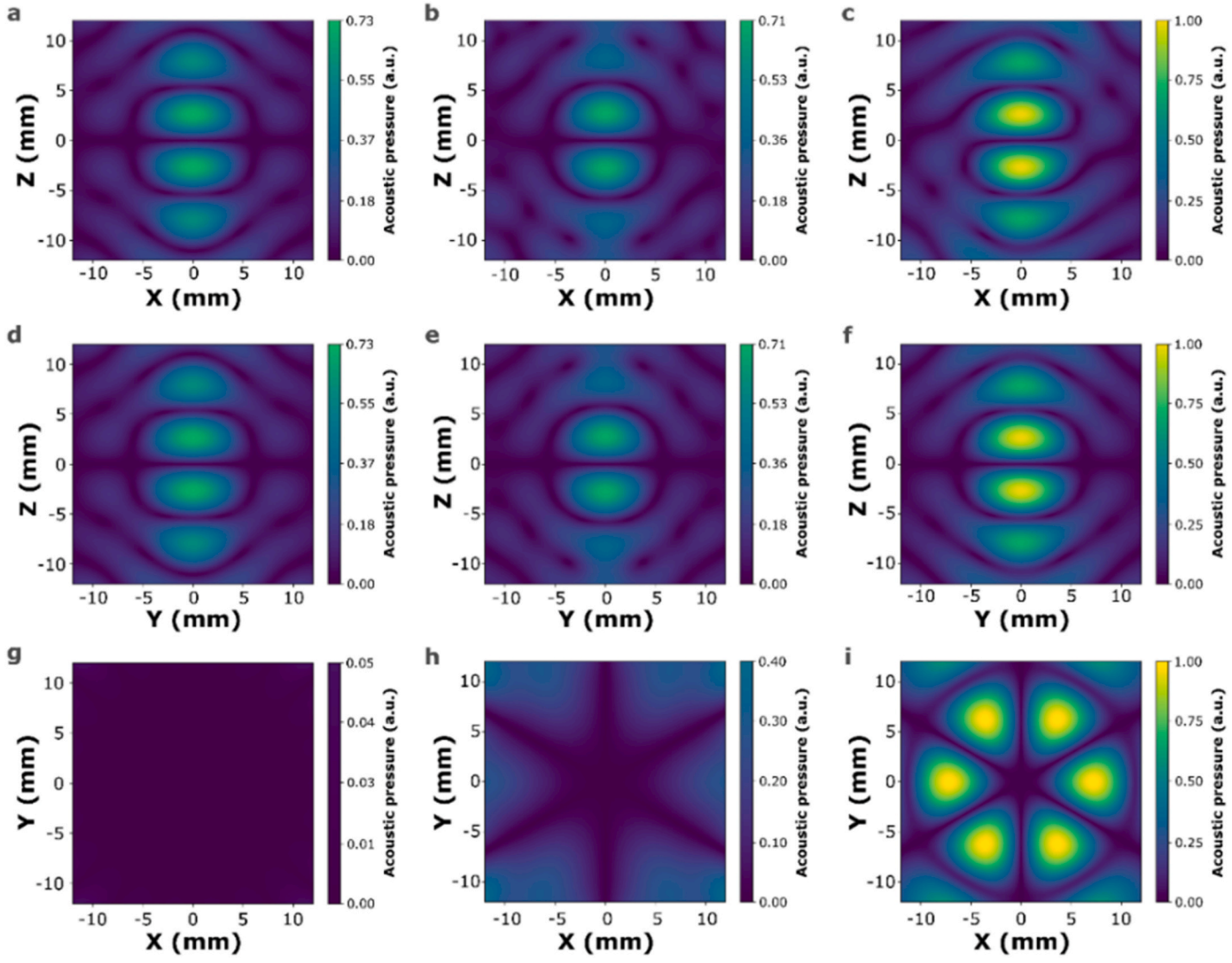


**Fig. 3.** Acoustic pressure fields along the (a–c) xz plane, (d–f) yz plane, and (g–i) xy plane at the central node (z = 0 mm), for levitators Mk1, Mk2, and Mk3, respectively, when operating in phase opposition, and with an operating frequency of transducers at 40 kHz. The values are normalized with respect to the maximum acoustic pressure of Mk3 along each plane. The maximum acoustic pressure on the xz and yz planes is the same; however, the acoustic pressure on the xy plane is lower by a factor of 7.5.

respectively. This matches well with respect to the percent difference of maximum acoustic pressure along the xz and yz planes, which indicates that the packing density plays a key role in that respect.

The magnitude of the acoustic pressure fields on the xy plane for each acoustic levitator are presented in Fig. 3d–f. It is observed that Mk1 showed 5% of the highest acoustic pressure generated by Mk3 (see Fig. 3g), followed by Mk2 at 40% (see Fig. 3h). Hence, acoustic levitator Mk3 presented significantly higher acoustic pressure along that plane, in comparison to the others. This indicates that Mk3 generates higher lateral forces, thus leading to a more confined acoustic trap (see Fig. 3i). To examine whether the presence of higher lateral forces in Mk3 is attributed to the higher opening angle, $\theta$, we simulated the acoustic pressure fields, along the xa, yz and xy planes (see Figs. S16a–c, Supporting Information), while also calculated the acoustic pressures along the x,y and z axes (see Figs. S16d–f, Supporting Information) without the presence of the upper, side transducers. Since 6 transducers were removed the total acoustic pressure would be reduced; hence to compensate for the loss of pressure we increased the parameter $p_0$ from 1.0 to 1.5. As a result, the highest acoustic pressure along the z and y axes remained approximately the same (see Fig. S16d and Fig. S16f, Supporting Information, respectively), thus we were able to compare only the lateral forces. In Fig. S16e, Supporting Information, it is evident that the lack of side transducers reduced the maximum acoustic pressure by 36%, which verified the hypothesis.

The simulations constitute a preliminary tool for visualizing the acoustic pressure field of the levitators when no object is levitated. Depending on the density and shape of the sample the reflected acoustic waves on the surface of the object will influence the acoustic radiation force field. The *levitate* Python framework offers the capability of simulating the acoustic radiation forces on different materials. In Fig. S6 and Fig. S7, Supporting Information, we have simulated the acoustic radiation force fields for a polystyrene bead with a diameter of 1 mm, based on the assumptions applied on the calculation of the Gor'kov potential (see Eq. (2) - Eq. (5)). It is observed that the acoustic radiation force around the trap is equally strong for levitators Mk1 and Mk2, while the radiation force of Mk3 is twice as strong.

### 3.3. Experimental evaluation

#### 3.3.1. Effect of distance of opposing arrays

A designing parameter that can be easily adjusted after 3D-printing the scaffold of a multiple-transducer acoustic levitator is the distance of opposing arrays. Recently, it was shown that by fine-tuning the distance of opposing arrays it is possible to increase the acoustic pressure near the acoustic node and consequently the levitation capacity [26]. This can be advantageous for the study of heavier objects; however, it may not be optimum, in the contact-free study of chemical solutions with ultra-low surface tension.

To investigate this, we used acoustic levitator Mk3 due to its high performance, and ease to place and levitate a sample. Initially, we calculated the theoretical acoustic pressure and acoustic radiation net force at the anti-node, in the case of $\Delta\varphi = \pi$ rad, for different distances of opposing arrays using the Python library *levitate* [28]. Fig. 4a, shows that the theoretically highest acoustic pressure is found for a distance of opposing arrays of approximately 38.6 mm. Following, we simulated the acoustic radiation force applied on a spherical levitated particle with a diameter of 1 mm, in accordance with Sapozhnikov and Bailey [30] as formulated in Ref. [27], with respect to the distance of opposing arrays. In that case we predicted that acoustic levitator Mk3 will present the highest acoustic radiation force at a distance of opposing arrays of 44.6 mm.

This was experimentally evaluated by monitoring the current consumption of acoustic levitator Mk3 (when $\Delta\varphi = \pi$ rad), in accordance with Contreras and Marzo [26], and the vertical position and aspect ratio of levitated water droplets while we varied the distance of opposing arrays. In Ref. [26], the acoustic pressure was evaluated

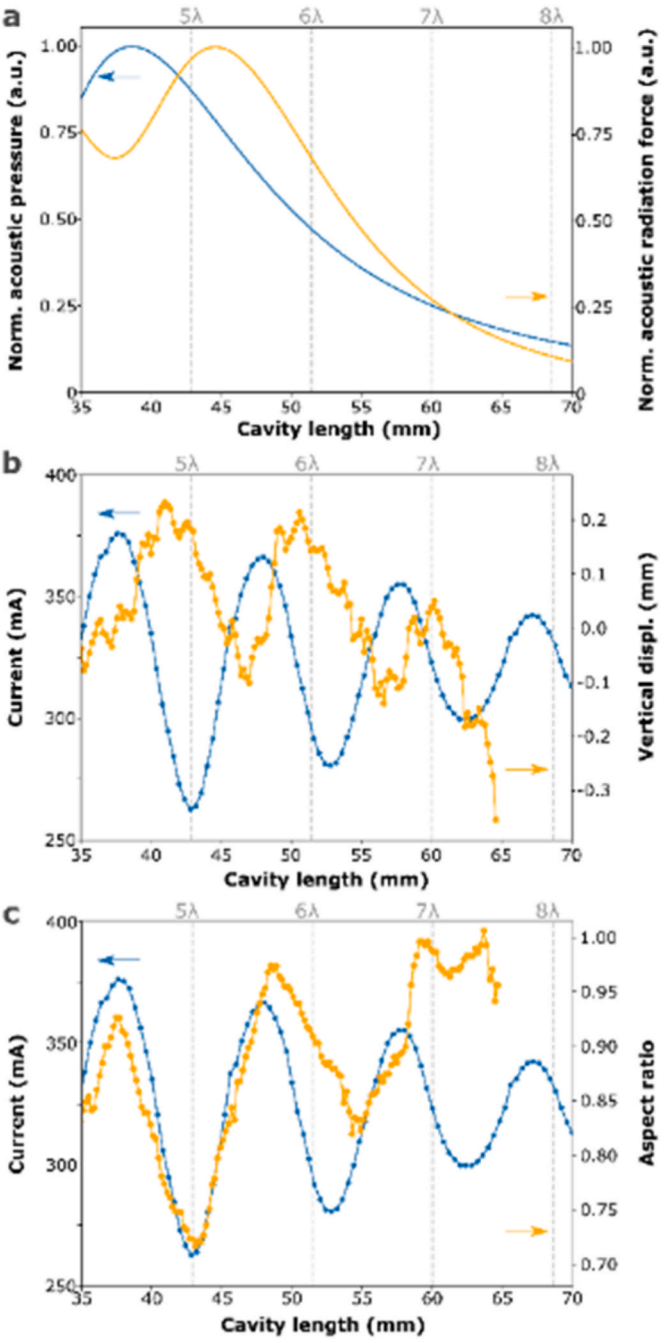


**Fig. 4.** a) Simulations of maximum acoustic pressure on the anti-node (left y-axis, blue line) generated by Mk3 and acoustic radiation net force on the anti-node applied on a polystyrene bead with diameter 1 mm (right, y-axis, orange line), b) current consumption of levitator Mk3, at 9.5 V, operating frequency of transducers at 40 kHz (left y-axis, blue line), and vertical displacement of a water droplet, with an initial volume of 2 μL (right, y-axis, orange line) with respect to the distance of opposing arrays, and c) current consumption of levitator Mk3, at 9.5 V, operating frequency of transducers at 40 kHz (left y-axis, blue line), and aspect ratio of a water droplet, with an initial volume of 2 μL (right, y-axis, orange line) with respect to the distance of opposing arrays.

through a schlieren deflectometer and the current consumption, where low consumption was associated with higher acoustic pressure. The vertical position was chosen as a study parameter because it is reported to be correlated with the acoustic radiation force [34,35]. Specifically, it was shown that the lower the acoustic radiation force applied on the object, the lower its position in space. Furthermore, in accordance with

Apfel *et al.* [34,35] the droplets tend to be spherical when low acoustic pressure is applied, and as the acoustic pressure is increased the droplets acquire an oblate shape. This is also justified by the fast that the lateral forces are 7.5–20 times lower than the vertical forces (see Fig. 3). Therefore, the aspect ratio can be used as a proxy for the amplitude of the acoustic radiation net force. We defined the aspect ratio as the height/width ratio; hence the more oblate the droplet is, as the applied acoustic pressure increases, the lower the aspect ratio.

In Fig. 4b it is observed that the current consumption of Mk3 and the vertical position of the water droplets with respect to the distance of opposing arrays follow the same damping oscillation. The changes in vertical displacement were in the range of ±0.2 mm and we observed that the levitated object moved upwards when the current consumption decreased and downwards when the current consumption of Mk3 increased. The highest vertical position was recorded when the distance of opposing arrays was 40.5 mm, which is 1.9, and 4.1 mm away from the distance of opposing arrays that corresponds to the simulated maximum acoustic pressure, and radiation force, respectively. The droplet ceased to levitate when the distance of opposing arrays was approximately 64 mm due to insufficiently high acoustic radiation forces to keep it levitating. This is in line with the simulations in Fig. 4a because at these distances of opposing arrays the acoustic pressure and radiation forces have exponentially decayed.

In Fig. 4c, we observe that the aspect ratio of the water droplets follows a similar damping oscillation pattern as one of the current consumption and the vertical displacement. As the distance of opposing arrays increased, the droplet became more spherical, leading to an aspect ratio close to 1. The maximum droplet deviation from sphericity (lowest aspect ratio) is observed at a distance of opposing arrays of approximately 43 mm, which matches the chosen distance of opposing arrays of the design. This value deviates 4.4, and 1.6 mm from the simulated maximum acoustic pressure and radiation force, respectively; however, it matches the minimum current consumption. Above 43 mm, a mismatch between the peaks of the current consumption, and the ones of the displacement and aspect ratio began to appear. This may be attributed to the gradual decrease of acoustic radiation force on the droplet, leading to a reduced influence on the droplet. We repeated the measurements three times, and the same pattern was observed(Fig. S8, Supporting information).

In the work by Contreras and Marzo [26] the current consumption and a rainbow schlieren deflectometer were employed for monitoring the acoustic wave fronts [36]. Inspired by their results we plotted separately the real and imaginary parts of the acoustic pressure, and we found that the real part matches the oscillation pattern of the vertical position, while the imaginary part matches well the aspect ratio pattern (see Fig. S9, Supporting Information). However, this effect is outside the scope of this study, and would require dedicated investigation. Furthermore, in Ref. [26] low current consumption was associated with higher acoustic pressure, which is in line with the above presented results. Hence herein, we provide an additional means as a proxy of the acoustic radiation net force through monitoring the aspect ratio and vertical position of a levitated water droplet, through a camera, or in the case of the first parameter even with a bare eye. Following the droplet deformation while varying the distance of opposing arrays can lead to the optimum choice of distance between the two opposing transducer arrays, based on the application.

### 3.3.2. *Phase difference and distance of opposing arrays*

As mentioned, the phase difference between the two opposing halves will affect the wave interactions. We experimentally investigated the effect of phase difference on the frequency response and performance of the acoustic levitators by measuring the current consumption with respect to the distance of opposing arrays and operating frequency. This experiment was performed with acoustic levitator Mk3 while operating in phase ($\Delta\varphi = 0$ rad) and in phase opposition ($\Delta\varphi = \pi$ rad). Fig. 5a shows that alternating the phase difference by π rad, shifts the damping oscillation pattern of the current consumption by $\lambda/2$. This verifies that changing the phase by π rad, is equivalent to shifting the algebraic sign of the signal. In the case where the two halves operated in phase ($\Delta\varphi = 0$ rad), the minimum current consumption was found at approximately 47 mm, while the maximum was at 43 mm. As showed in Fig. 4, the highest radiation force was found when the current consumption reached a minimum. This indicates that to optimally operate Mk3 in the case of no phase difference ($\Delta\varphi = 0$ rad), the distance of opposing arrays needs to be set at 47 mm. Hence, by altering the phase difference between the two halves, the performance of the levitator will change. This also implies that for a constant distance of opposing arrays and voltage, the acoustic pressure applied on a levitated object can be controlled by properly adjusting the phase of the transducers. The advanced control of phased arrays has found application in holography [20], and in the levitation of objects larger than the wavelength of the acoustic waves [37].

### 3.3.3. *Effect of the operating frequency of transducers*

In all the measurements presented above, the transducers were operating at their resonant frequency of 40 kHz, in accordance with [31]. To investigate further on the wave interactions, we varied the operational frequency of the transducers, through Arduino, from 36 to

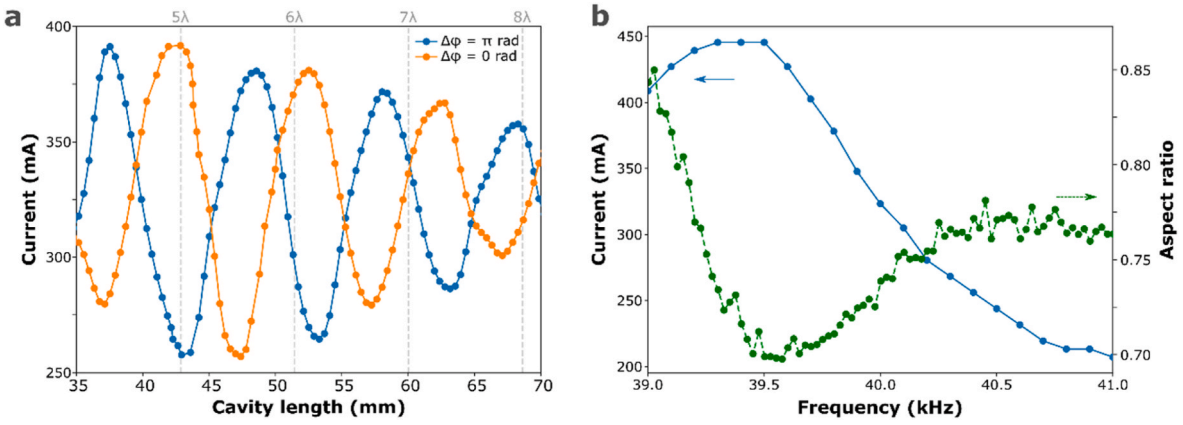


**Fig. 5.** a) Current consumption of the acoustic levitator Mk3 and Arduino, when operating in phase opposition ($\Delta\varphi = \pi$ rad, blue line), and in phase ($\Delta\varphi = 0$ rad, orange line), at 9.5 V, and operating frequency of the transducers was 40 kHz, b) current consumption of acoustic levitator Mk3 and Arduino with respect to the operating frequency of the transducers, while in phase opposition (left y-axis, blue line), aspect ratio of a water droplet with volume of 3.45 μL (right y-axis, green dotted line) with respect to the operational frequency of the transducers, while the levitator halves were operating in phase opposition ($\Delta\varphi = \pi$ rad). The distance of opposing arrays of Mk3 was 43 mm, and the operating voltage was 9.5 V.

41 kHz and the current consumption was recorded in the cases where the two halves were opposing and not opposing each other. The measurements were repeated for the case where the halves were in phase, and in phase opposition. When the two halves were not interacting, the current consumption with respect to the operational frequency was the same regardless of the phase difference (see Fig. S11, Supporting Information). Whilst, as shown in Fig. S12, Supporting Information, the current consumption pattern presented different minima and maxima depending on the phase difference, for the same distance of opposing arrays and voltage. Hence, the different patterns observed in Fig. S12, Supporting Information are attributed to the interactions between the piezoelectric transducers which in response influenced their current consumption. It is also observed that for the case of phase opposition, the current consumption of acoustic levitators Mk1, Mk2, and Mk3 was matching the local maximum of the operating frequency response of the transducers, at 39.5 kHz. However, this value is below the resonant frequency of the transducers (40 kHz, in accordance with [31]).

To examine whether the performance of the device is influenced by this frequency shift, we levitated a water droplet and measured the aspect ratio and vertical position, while varying the operating frequencies of levitator Mk3 within the range of 39–41 kHz. The current consumption was also monitored through the Arduino Uno board. In Fig. 5b, we observe that the aspect ratio of the water droplet reached a local minimum when the operating frequency reached the local maximum at 39.5 kHz. Furthermore, we show that although the current consumption at 39.1 kHz and 39.6 kHz is equal to 427 mA, the aspect ratio of the water droplet was 0.81 and 0.72. This 11% difference in droplet aspect ratio is attributed to the fact that the operating frequency begins to deviate significantly from the manufacturing resonant frequency of the transducers, thus reducing rapidly the emission amplitude of the transducers. The measurements were repeated three times with water droplets of different volumes and the same pattern was observed (see Fig. S13a, Supporting Information). In Fig. S13b, Supporting Information, it is shown that the droplets moved upwards when the frequency increased, which is related to the change in the generated acoustic wavelength generated of the transducers. Overall, we showed that it is possible to further improve the performance of the levitator by changing the operating frequency, however the operating frequency should not deviate more than 1 kHz away from the resonant frequency of the transducers, or the transducers will lose in radiation amplitude. Since the accuracy of the 3D printed acoustic levitators is in the range of $\pm 1$ mm, this fine-tuning can optimize the performance without changing the distance of opposing arrays.

### 3.3.4. Levitation capacity

The levitation capacity, $C_{\text{lev}}$ (see Eq. (6)) quantifies empirically the levitation strength of an acoustic levitator and allows the direct comparison between them. The advantages of utilizing a solid object are that the weight does not vary over time and it cannot be deformed as opposed to a volatile liquid, thus affecting the acoustic pressure field in the same way throughout the measurement. Table 2, shows the lowest recorded voltages required, by each acoustic levitator, to levitate the silica bead along the vertical and horizontal configuration. In all cases a silica bead of 7 mg in mass was used, except for TinyLev in the horizontal configuration, where a 1 mg silica bead was levitated, due to insufficiently high lateral forces to perform the measurements. These masses correspond to a weight of 68.6 μN and 9.8 μN, respectively. Through the levitation capacity parameter we determine the voltage at which these threshold forces were reached for each acoustic levitator. As a result, the lower the minimum voltage, the higher the levitation capacity.

**Table 2**
Experimental records of the voltage at which the silica bead was dropped by each acoustic levitator when the device was operating in the vertical and horizontal configuration. In all cases, the levitator halves were in phase opposition ($\Delta\varphi = \pi$ rad), and the operating frequency of the transducers was set at 40 kHz * For TinyLev the mass of the silica bead was 1 mg, in horizontal configuration.

| Configuration/Voltage (V) | TinyLev* | Mk1 | Mk2 | Mk3 |
|---|---|---|---|---|
| **Vertical configuration** | 11.1 ± 0.1 | 9.3 ± 0.1 | 8.9 ± 0.1 | 6.5 ± 0.1 |
| **Horizontal configuration** | 7.1 ± 0.1 | 20.8 ± 0.1 | 20.5 ± 0.1 | 14.4 ± 0.1 |

In Fig. 6a, the levitation capacity, $C_{\text{lev}}$ of each acoustic levitator is plotted. It is evident that all new designs perform better than TinyLev in both horizontal and vertical configurations. Levitators Mk1 and Mk2 had similar levitation capacity, although Mk2 was operating on 20 transducers less than Mk1. This is supported by the simulations (see Fig. 3) that show similar maximum acoustic pressure and acoustic radiation force for these two designs. Levitator Mk3 presented 3.5 and 1.7 times higher levitation capacity than TinyLev, along the horizontal and vertical configurations, respectively. In comparison to Mk1 and Mk2, the acoustic levitator Mk3 showed on average 1.4 times higher levitation capacity along both configurations. Overall, the vertical levitation capacity correlates well to the packing density of transducers, as Mk3 is more densely packed than TinyLev by approximately 56%, and 30% for Mk1 and Mk2, which is close to the percent difference of levitation capacity. Regarding the horizontal levitation capacity, it is the opening angle that appears to have the main influence, as the higher the opening angle, $\theta$, the larger the lateral forces and the higher the horizontal levitation capacity of a levitator (see Fig. S16, Supporting Information).

This empirical metric clearly demonstrates the difference in performance among the levitators and allows a direct comparison between them; however, the choice of normalizing the weight by the drop-of voltage is certainly not sufficient to grant the relationship between acoustic pressure and driving voltage. Instead, we recorded the aspect ratio of water droplets (volume 2–2.5 μL) with respect to the driving voltage in the range of 6.5–23 V for Mk1 and a linear relationship was observed (Fig. S15, Supporting Information). One practical limitation of this metric is that the overall voltage of the driving circuit has a lower limit of 5 V which is required for operating the Arduino Uno board. However, this can be solved by levitating heavier objects.

Next, we simulated the trap stiffness of each acoustic levitator. This parameter relates to the resistance a levitated object will experience while being displaced in an acoustic pressure field. Hence, if an acoustic levitator presents high trap stiffness, then the levitation capacity is expected to be high. In Fig. 6b we observe that acoustic levitator Mk3 presents the highest trap stiffness along the horizontal and vertical axis, following by Mk1, Mk2, and TinyLev. These theoretical results correlate well to the experimental ones obtained through the levitation capacity metric.

### 3.3.5. Evaluation of the spatial stability

The spatial stability of the levitated sample is an important factor that can influence the degree of experimental error while capturing images or performing other measurements on self-standing droplets or solid objects. This will depend on the strength and the pattern of the acoustic pressure field around the node, that results from the designing parameters presented previously. These parameters relate to the trap stiffness and the presence of curl forces [38]. Using liquid droplets for these measurements allowed the examination of potential dependencies between the volume of the droplet and the stability along the vertical and horizontal directions. Fig. 6c–d shows the average horizontal, and vertical displacement of water droplets (volume range: 0.5–5 μL, Fig. S17, Fig. S18, Fig. S19, Fig. S20 Supporting Information) over a period of 10 min for each acoustic levitator, at different driving voltages. The lowest voltage was initially chosen to be 7 V; however, with TinyLev and Mk2 the lowest voltage at which reproducible measurements could be collected was 10 V, and 7.5 V, respectively. It is observed that levitator Mk3 presented the least droplet displacement, hence the highest stability, in relation to both vertical and horizontal displacement. Following, levitator Mk2 presented lower stability along the horizontal displacement and similar stability in comparison to Mk1. From Fig. S19

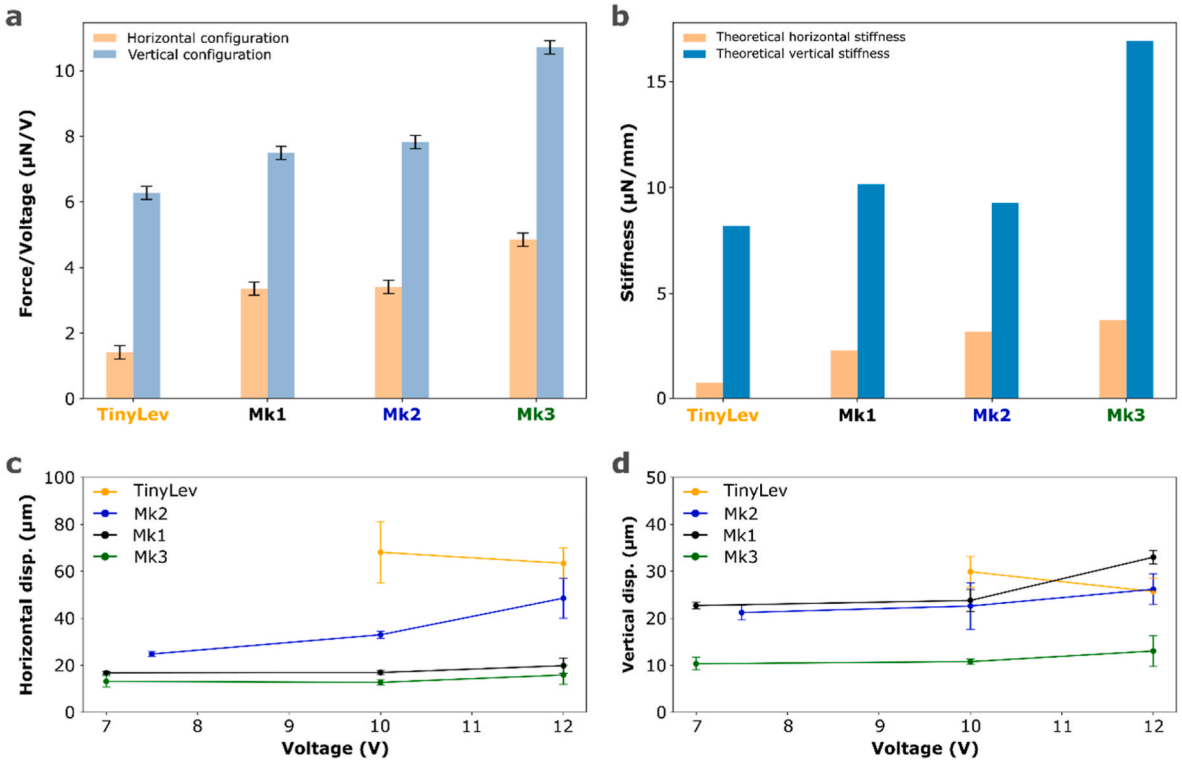


**Fig. 6.** a) Levitation capacity of acoustic levitators TinyLev, Mk1, Mk2, and Mk3 expressed as force over voltage, b) Simulated trap stiffness of acoustic levitators along the horizontal xy plane (orange) and the vertical xz and yz planes (blue), and stability of levitated water droplets, expressed as average displacement of droplet over a period of 10 min along the c) horizontal axis x, and d) vertical axis z, when the opposing levitator halves were operating in phase opposition ($\Delta\varphi = \pi$ rad), and the operating frequency of the transducers was 40 kHz.

and Fig. S20 Supporting Information, we observe that acoustic levitator Mk2 presented higher levels of horizontal and vertical displacement for water droplets with volume lower than 2 μL. This may have occurred due to resonance between the acoustic waves and the levitated object, thus causing it to oscillate.

Overall, Mk3 was 3.7 and 1.4 times better than TinyLev, 0.3 and 1.3 better than Mk1, and 1.5 and 1.1 times better than Mk2, along the horizontal and vertical stability, respectively. The precise gains for each voltage are shown in Tables S1, S2, and S3, Supporting Information, for TinyLev, Mk1, and Mk2, respectively.

## 4. Open-source software for designing and constructing customized acoustic levitators

Depending on the target application a unique design may be required. To facilitate the design and fabrication of customized acoustic levitators we built an open-source, interactive software that computes the acoustic pressure and acoustic radiation force fields of acoustic levitators with different parameters related to the design (*e.g.*, number of transducers, distance of opposing arrays, *etc.*), and the type of ultrasonic transducers. The software is based on Python which is an open-source, versatile, and flexible programming language, which allows easy adjustment of the code. Additionally, the user can export files suitable for 3D printing where the desirable positions of the ultrasonic transducers are designated. The code and further instructions are available on https://git.chalmers.se/bordes/omnilev.

## 5. Conclusion

In contrast to the Langevin horn, multiple-transducers acoustic levitators offer high flexibility in terms of design and resulting performance, thus allowing the customization of the device for specific applications. Herein, we reported and examined the key designing principles that affect the performance of single-axis, multiple-transducers acoustic levitator. We initially simulated the customized acoustic levitators in terms of acoustic pressure and acoustic radiation force fields. Following, we 3D printed and constructed the devices, and then evaluated them experimentally.

The three new designs showed better experimental performance in terms of levitation capacity and stability than TinyLev. Furthermore, we showed through simulations and experimental results that by fine-tuning the designing parameters, it is possible to create levitators that are compact, yet still able to generate similar acoustic pressure to levitators with more transducers, as in the case of Mk1 and Mk2; however, they varied in terms of stability, which was attributed to a volume dependency effect and potential resonance between the droplet size and the pressure applied on it. A recent publication by Contreras and Volke-Sepúlveda [39] showed that by properly adjusting the phased arrays, further improvements in terms of stability and levitation capacity can be achieved. The similar levels of acoustic pressure and levitation capacity in Mk1 and Mk2 were mainly attributed to the packing density, and the opening angle. Simultaneously, it is evident that for smaller radius of curvature, as in the case of Mk2, one needs to choose a smaller distance between the arrays. Hence, the radius of curvature needs to be considered when choosing an appropriate field of view for a certain application. The simulations were used as a preliminary, guiding tool to design new configurations. The absolute prediction of highest acoustic pressure and radiation net force with respect to the distance of opposing arrays was more challenging. However, the distance of opposing arrays can be easily adjusted after 3D printing, so that the acoustic radiation force is optimum depending on the experimental demands, while further fine-tuning of acoustic radiation net force can be achieved by adjusting the operational frequency of the transducers within limits.

Furthermore, our results were in line with the study done by Contreras and Marzo [26], in which the current consumption was used as a proxy to determine the optimum distance of opposing arrays, while we

provided an additional means for the evaluation of the resulting acoustic radiation net force through the deformation of a water droplet. In terms of applications, acoustic levitator Mk1 was employed for the study of surface tension of surfactant solutions [7], while Mk2 may be suitable for studies related to mixing of solutions, fluid flow dynamics or solid-state NMR. Acoustic levitator Mk3 is unique due to the close packing of transducers in a hexagonal arrangement, which led to the highest stability and levitation strength among all designs. These characteristics are important in applications related to spectroscopical techniques where high-level control of the levitated samples displacement is crucial.

Overall, we expect that this analysis will facilitate the implementation of acoustic levitation in various fields of research, and we aspire that the open-source software will encourage more researchers to use this technique. Future development tracks lean towards the implementation of a controlled phase management to control the rotation of spherical and oblate levitated objects.

## CRediT authorship contribution statement

**Smaragda-Maria Argyri:** Data curation, Formal analysis, Investigation, Methodology, Validation, Visualization, Writing – original draft, Writing – review & editing, Software. **Carl Andersson:** Software, Validation, Visualization, Writing – review & editing, Methodology. **Nicolas Paillet:** Investigation, Software. **Lars Evenäs:** Funding acquisition, Resources, Supervision. **Jens Ahrens:** Writing – review & editing, Methodology. **Asier Marzo:** Validation, Writing – review & editing. **Víctor Contreras:** Validation, Writing – original draft, Writing – review & editing. **Romain Bordes:** Conceptualization, Data curation, Funding acquisition, Investigation, Resources, Supervision, Writing – original draft, Writing – review & editing.

## Declaration of competing interest

The authors declare that they have no known competing financial interests or personal relationships that could have appeared to influence the work reported in this paper.

## Acknowledgements

The authors are grateful for the financial support from the Swedish Research Council (VR) (Public, Sweden), and the Swedish Foundation for Strategic Research (SSF) (Non-Profit, Sweden).

## Appendix A. Supplementary data

Supplementary data to this article can be found online at https://doi.org/10.1016/j.jsamd.2024.100720.

## References

[1] D. Zang, K. Lin, L. Li, Z. Chen, X. Li, X. Geng, Acoustic levitation of soap bubbles in air: beyond the half-wavelength limit of sound, Appl. Phys. Lett. 110 (12) (2017).
[2] Q. Shi, W. Di, D. Dong, L.W. Yap, L. Li, D. Zang, W. Cheng, A general approach to free-standing nanoassemblies via acoustic levitation self-assembly, ACS Nano 13 (5) (2019) 5243–5250.
[3] D. Zang, J. Li, Z. Chen, Z. Zhai, X. Geng, B.P. Binks, Switchable opening and closing of a liquid marble via ultrasonic levitation, Langmuir 31 (42) (2015) 11502–11507.
[4] Z. Tang, S. Lin, Z.L. Wang, Quantifying contact-electrification induced charge transfer on a liquid droplet after contacting with a liquid or solid, Adv. Mater. 33 (42) (2021) 2102886.
[5] S.J. Brotton, R.I. Kaiser, Controlled chemistry via contactless manipulation and merging of droplets in an acoustic levitator, Anal. Chem. 92 (12) (2020) 8371–8377.
[6] L. Cohen, M.I. Quant, J.D. Don, Real-time measurements of pH changes in single, acoustically levitated droplets due to atmospheric multiphase chemistry, ACS Earth Space Chem. 4 (6) (2020) 854–861.
[7] S.M. Argyri, L. Evenäs, R. Bordes, Contact-free measurement of surface tension on single droplet using machine learning and acoustic levitation, J. Colloid Interface Sci. 640 (2023) 637–646.
[8] S. Mohanty, I.S. Khalil, S. Misra, Contactless acoustic micro/nano manipulation: a paradigm for next generation applications in life sciences, Proceedings of the Royal Society A 476 (2020) 20200621.
[9] S. van Waser, Y. You, S. Beck, J. Riedel, D.A. Volmer, Miniaturized protein digestion using acoustic levitation with online high resolution mass spectrometry, Anal. Chem. 95 (8) (2023) 4190–4195.
[10] J. Li, W.D. Jamieson, P. Dimitriou, W. Xu, P. Rohde, B. Martinac, M. Baker, B. W. Drinkwater, O.K. Castell, D.A. Barrow, Building programmable multicompartment artificial cells incorporating remotely activated protein channels using microfluidics and acoustic levitation, Nat. Commun. 13 (1) (2022) 4125.
[11] N. Jeger-Madiot, L. Arakelian, N. Setterblad, P. Bruneval, M. Hoyos, J. Larghero, J.-L. Aider, Self-organization and culture of Mesenchymal Stem Cell spheroids in acoustic levitation, Sci. Rep. 11 (1) (2021) 8355.
[12] D. Ensminger, L.J. Bond, Ultrasonics: Fundamentals, Technologies, and Applications, CRC press, 2011.
[13] R.H. Morris, E.R. Dye, P. Docker, M.I. Newton, Beyond the Langevin horn: transducer arrays for the acoustic levitation of liquid drops, Phys. Fluids 31 (10) (2019) 101301.
[14] A. Stindt, M. Andrade, M. Albrecht, J. Adamowski, U. Panne, J. Riedel, Experimental and numerical characterization of the sound pressure in standing wave acoustic levitators, Rev. Sci. Instrum. 85 (1) (2014) 015110.
[15] W. Oran, L. Berge, H. Parker, Parametric study of an acoustic levitation system, Rev. Sci. Instrum. 51 (5) (1980) 626–631.
[16] W. Xie, C. Cao, Y. Lü, B. Wei, Levitation of iridium and liquid mercury by ultrasound, Phys. Rev. Lett. 89 (10) (2002) 104304.
[17] Z. Hong, W. Xie, B. Wei, Acoustic levitation with self-adaptive flexible reflectors, Rev. Sci. Instrum. 82 (7) (2011) 074904.
[18] Y.H.T. Ochiai, J. Rekimoto, Three-dimensional mid-air acoustic manipulation by ultrasonic phased arrays, PLoS One 9 (5) (2014) e97590.
[19] A. Watanabe, K. Hasegawa, Y. Abe, Contactless fluid manipulation in air: droplet coalescence and active mixing by acoustic levitation, Sci. Rep. 8 (1) (2018) 10221.
[20] A. Marzo, S.A. Seah, B.W. Drinkwater, D.R. Sahoo, B. Long, S. Subramanian, Holographic acoustic elements for manipulation of levitated objects, Nat. Commun. 6 (1) (2015) 8661.
[21] T. Omirou, A. Marzo, S.A. Seah, S. Subramanian, LeviPath: modular acoustic levitation for 3D path visualisations, in: 33rd Annual ACM Conference on Human Factors in Computing Systems, 2015.
[22] Y. Ochiai, T. Hoshi, J. Rekimoto, Pixie dust: graphics generated by levitated and animated objects in computational acoustic-potential field, ACM Trans. Graph. 33 (4) (2014) 1–13.
[23] W.A. Oran, L.H. Berge, H.W. Parker, Parametric study of an acoustic levitation system, Rev. Sci. Instrum. 51 (5) (1980) 626–631.
[24] A. Marzo, A. Ghobrial, L.a.C.M. Cox, A. Croxford, B. Drinkwater, Realization of compact tractor beams using acoustic delay-lines, Appl. Phys. Lett. 110 (1) (2017) 014102.
[25] A. Marzo, A. Barnes, B.W. Drinkwater, TinyLev: a multi-emitter single-axis acoustic levitator, Rev. Sci. Instrum. 88 (8) (2017) 085105.
[26] V. Contreras, A. Marzo, Adjusting single-axis acoustic levitators in real time using rainbow schlieren deflectometry, Rev. Sci. Instrum. 92 (1) (2021) 015107.
[27] C. Andersson, Sound field design for transducer array-based acoustic levitation, PhD theses, Chalmers Tekniska Hogskola (Sweden) (2022).
[28] C. Andersson, Python implementation of acoustic levitation and related topics, GitHub (26 October 2022) [Online], https://github.com/AppliedAcousticsChalmers/levitate. (Accessed 2 November 2022).
[29] C. Andersson, J. Ahrens, Minimum trap separation for acoustical levitation using phased ultrasonic transducer arrays, in: 23rd International Congress on Acoustics, 2019. Aachen, Germany.
[30] O.A. Sapozhnikov, M.R. Bailey, Radiation force of an arbitrary acoustic beam on an elastic sphere in a fluid, J. Acoust. Soc. Am. 133 (2) (2013) 661–676.
[31] 40khz Plastic Case Ultrasonic Transducer Long Distance Sensor," Manorshi, [Online]. Available: https://www.manorshi.com/40khz-Plastic-Case-Ultrasonic-Transducer-Long-Distance-Sensor-pd42358866.html. [Accessed 15 January 2024].
[32] J. Canny, A computational approach to edge detection, IEEE Trans. Pattern Anal. Mach. Intell. (6) (1986) 679–698.
[33] Doxygen, "OpenCV," OpenCV, Online, https://docs.opencv.org/4.x/d3/dc0/group__imgproc__shape.html#gadf1ad6a0b82947fa1fe3c3d497f260e0, 2022. (Accessed 12 May 2023).
[34] Y. Tian, R.G. Holt, R.E. Apfel, Deformation and location of an acoustically levitated liquid drop, J. Acoust. Soc. Am. 93 (6) (1993) 3096–3104.
[35] W.T. Shi, R.E. Apfel, Deformation and position of acoustically levitated liquid drops, J. Acoust. Soc. Am. 99 (4) (1996) 1977–1984.
[36] T. Azuma, T. Akihiro, S.-I. Umemura, Observation of ultrasonic wavefronts by synchronous Schlieren imaging, Jpn. J. Appl. Phys. 41 (5) (2002) 3308–3312.

[37] C. Andersson, Acoustic levitation of multi-wavelength spherical bodies using transducer arrays of non-specialized geometries, J. Acoust. Soc. Am. 151 (5) (2022) 2999–3006.
[38] C. Andersson, J. Ahrens, Reducing spiraling in transducer array based acoustic levitation, in: IEEE International Ultrasonics Symposium (IUS), Las Vegas, Nevada, USA, 2020.
[39] V. Contreras, K. Volke-Sepúlveda, Enhanced standing-wave acoustic levitation using high-order transverse modes in phased array ultrasonic cavities, Ultrasonics (2024) 107230.